

Numerically Efficient Degradation Model of Catalyst Layers in PEM Fuel Cells using Modelica

Jakob Träger¹ Steffen Heinke¹ Wilhelm Tegethoff¹ Jürgen Köhler¹

¹Institut für Thermodynamik, TU Braunschweig, Germany, {j.traegner, s.heinke, w.tegethoff, j.koehler}@tu-braunschweig.de

Abstract

Degradation of the catalyst layer is a major challenge for the commercialization of polymer electrolyte membrane fuel cells (PEMFCs). Numerical modeling helps to understand and analyze the degradation phenomena, to transfer results from accelerated stress tests (ASTs) to real applications and to optimize operating conditions regarding degradation. We implemented a typical catalyst degradation model for platinum used in literature in Modelica. A numerical analysis shows the problem of “stiffness” for these models, meaning the tremendous difference in time constants. Assuming the platinum ion concentration in the ionomer to be in quasi-equilibrium helps to reduce the “stiffness”, increases simulation speed and numerical robustness without any relevant inaccuracy. For a typical AST, the simulation speed can be more than doubled ending in a real-time factor of over 1,000. Thus, 500 hours of AST can be simulated within less than 30 minutes, which gives room for extensive analysis with the model.

Keywords: PEM Fuel Cells, Catalyst Degradation, Stiff System, Time Constants, quasi-equilibrium

1 Introduction

Polymer electrolyte membrane fuel cells (PEMFCs) are a promising technology which provides locally CO₂-free electrical energy. Their usage, e.g. in electric aircraft or fuel cell electric vehicles (FCEVs) can contribute to the announced aim of climate neutrality (European Union 2021).

PEMFCs use hydrogen at the anode and oxygen at the cathode to produce water, electrical energy and heat through the hydrogen oxidation reaction (HOR) and oxygen reduction reaction (ORR):

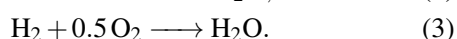
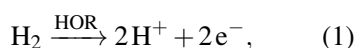


Figure 1 shows a schematic PEMFC. The HOR and ORR take place at the catalyst layers (CLs), which are placed on the membrane. In commercial PEMFCs, platinum or platinum alloys are used as catalyst material. Besides the catalyst particles, the CL consists of a porous

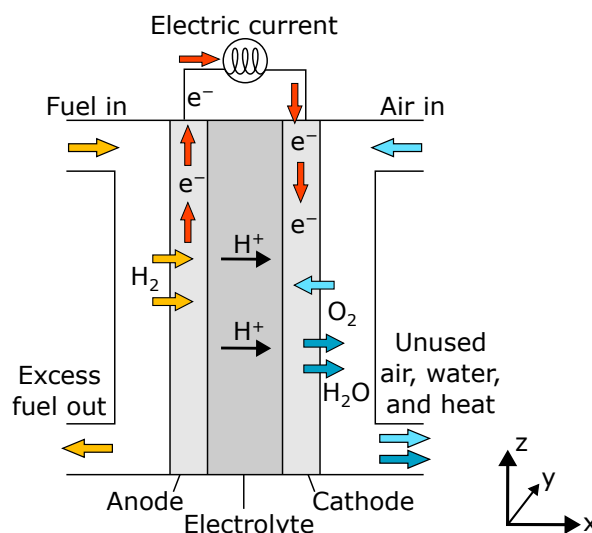
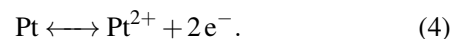


Figure 1. Schematic illustration of a PEMFC (Figure based on *Proton Exchange Fuel Cell Diagram* by Mattucci licensed under CC0 1.0 Universal Public Domain Dedication)

support material, typically carbon, and the ionomer. The latter allows the transport of protons.

Platinum is costly and its degradation is a main contributor to PEMFC performance loss (Borup et al. 2020). To reduce costs and nevertheless keep the efficiency high, very small platinum particles in the range of nanometres are used, which have a high surface area to mass ratio. Those small particles are known to be less stable than bulk material and, hence, more prone to electrochemical platinum dissolution:



Platinum ions (Pt²⁺) migrate through the ionomer to larger particles. That is why smaller particles are getting smaller and finally completely dissolute, while larger particles are growing. The size dependency of the platinum dissolution (Gibbs-Thomson effect) leads to the so-called electrochemical Ostwald-Ripening (Wagner 1961; Shao-Horn et al. 2007). The platinum surface decreases for a constant platinum mass in the catalyst layer, since larger particles have a lower surface to mass ratio. Figure 2 shows a schematic representation of this phenomena. The reduced catalyst surface area leads to increased activation losses (Zihrul et al. 2016; Bernhard et al. 2023), increased

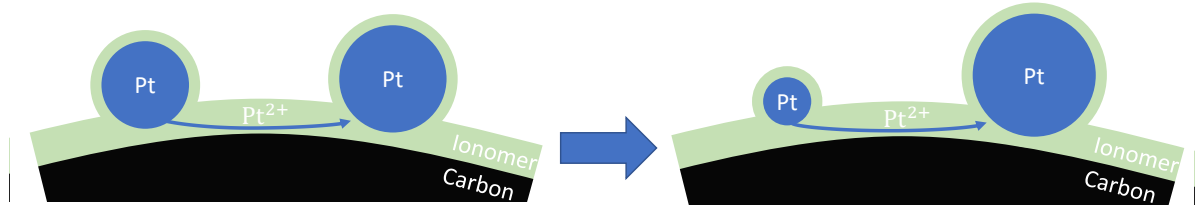


Figure 2. Schematic visualization of electrochemical Ostwald-Ripening. Smaller platinum particles are more prone to electrochemical dissolution, while platinum ions tend to re-deposit on larger particles. The increase of average particle size leads to a decreased platinum surface and accordingly lower cell voltage and fuel cell efficiency.

oxygen transport resistances in the catalyst layer (Greszler, Caulk, and Sinha 2012) and, hence, reduced cell voltage and efficiency.

Different groups have implemented catalyst degradation models for PEMFCs. Most of them use the kinetic model for platinum oxidation and dissolution initially proposed by Darling and Meyers (2003). Bi and Fuller (2008) and Darling and Meyers (2005) calculated the platinum dissolution not only for one but two particle groups with different radii which allowed to describe the reduction of electrochemical surface area (ECSA) for the first time. Later, Holby and Morgan (2012) calculated the platinum dissolution for a particle size distribution (PSD) approximated by several particle groups which allowed to describe the loss of ECSA more precisely. Li et al. (2015) used a similar model approach with a 1D through-plane (x -axis direction in figure 1) discretized CL. Schneider et al. (2019) added other degradation mechanisms like carbon corrosion and cathodic dissolution, i.e. dissolution during a reduction of potential, to the model. Jahnke et al. (2020) coupled the degradation model with a 2D along-the-channel (x and z -axis direction in figure 1) fuel cell model. Other contributions came from, among others, Rinaldo, Stumper, and Eikerling (2010), Zhang et al. (2013), Ahluwalia, Arisetty, Peng, et al. (2014), Kregar et al. (2019) and Prokop et al. (2019).

A lot of work was done with catalyst degradation models of the type based on Darling and Meyers (2003). However, to the best of the authors' knowledge, we present for the first time a numerical analysis for these kind of models and an implementation in the multi-physics modeling language Modelica. Assuming the platinum ion concentration to be in quasi-equilibrium, we propose a possibility to increase simulation speed and numerical robustness without relevant inaccuracies.

2 Modeling of Catalyst Degradation in PEM Fuel Cells

In the following section, the catalyst degradation model is described briefly to allow the reader to understand the differential equations. For the sake of simplicity, the following assumptions were made:

- Anodic platinum dissolution and, thus, Ostwald

ripening is the main irreversible degradation mechanism. Neither coalescence nor chemical dissolution of platinum oxide is part of the model.

- Platinum ion diffusion in the membrane can be neglected. Thus, no Platinum band is forming.
- Platinum oxidation can be described with a simple one-step reaction mechanism without size effect on platinum oxidation. Sub-surface oxide is not taken into account. Thus, no cathodic dissolution takes place.
- The catalyst is pure platinum and the geometric surface area of the spherical particles is equal to the ECSA.
- The CL can be described with a 0D model with a uniform platinum ion concentration in the ionomer. This assumption is justified due to high electric conductivity (electric potential as the main stressor) and the high ratio of catalyst surface to ionomer volume.

Platinum particles in the catalyst layers exist with different sizes forming a PSD, which can typically be approximated by using a log-normal distribution. Figure 3 shows the used PSD. It is approximated using 20 equidistant distributed particle groups between $r_1 = 0.75$ nm and $r_{20} = 3.5$ nm, where 20 is an arbitrary compromise between accuracy and simulation speed. The average diameter, standard deviation and platinum loading is based on the data from Jahnke et al. (2020), see appendix A. All particles in one group have the same radius and they shrink or grow due to electrochemical dissolution or re-deposition, which is called the radial evolution approach (Holby and Morgan 2012). The surface area of all particles can be described with the roughness factor rf (catalyst surface divided by geometric surface of the fuel cell) using the platinum loading L_{Pt}^i (platinum mass divided by geometric surface of the fuel cell) of each particle group i :

$$rf = \sum_{i=1} \left(\frac{3}{\rho_{Pt} r^i} L_{Pt}^i \right), \quad (5)$$

$$L_{Pt}^i = \frac{4}{3} \pi \rho_{Pt} t_{CL} (r^i)^3 n^i. \quad (6)$$

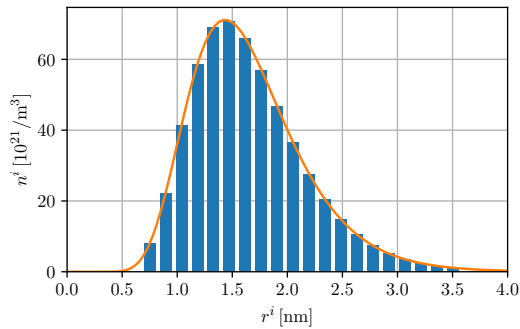


Figure 3. Initial PSD with continuous log-normal distribution and discrete particle groups

The radius r^i of a particle group changes due to Ostwald ripening. The volumetric specific number of particles n^i , the platinum density ρ_{Pt} and the catalyst thickness t_{CL} stay constant.

Platinum oxidation is assumed to follow the simple one step reaction proposed by Darling and Meyers (2003). Oxide coverage might dependent on the particle size. Ahluwalia, Arisetty, Wang, et al. (2013) measured an increasing coverage with particle size, while most models, including Darling and Meyers (2003), assume the opposite. That is why no dependency of the oxide coverage θ_{PtO} on the particle size is considered and the platinum oxide coverage can be described with one differential equation:

$$\frac{d\theta_{PtO}}{dt} = \frac{R_{PtO}}{\Gamma}, \quad (9)$$

where Γ is the number of active sites on a platinum surface and R_{PtO} is the reaction rate of platinum oxidation calculated according to equation 7. All parameters are listed in table 2.

The proton concentration c_{H^+} used in equation 7 is calculated, according to Darling and Meyers (2003), using the equivalent weight of the membrane EW , the density of the dry ionomer $\rho_{i,dry}$, the molar weight of water M_{H_2O} and its density ρ_{H_2O} :

$$c_{H^+} = \frac{1}{\frac{EW}{\rho_{i,dry}} + \frac{\lambda M_{H_2O}}{\rho_{H_2O}}}. \quad (10)$$

The water content λ is calculated according to Springer, Zawodzinski, and Gottesfeld (1991) and is only a function of relative humidity.

At high electric potential E , platinum tends to dissolve in the ionomer. The reaction rate for platinum dissolution R_{diss}^i is calculated according to equation 8. The higher the oxide coverage, the lower the platinum dissolution since the oxide protects the platinum. In the model, the surface fraction available for platinum dissolution θ_{av} is calculated by the simple relationship $\theta_{av} = \max(0, 1 - \theta_{PtO})$. The dissolution leads to an increase of platinum ion concentration $c_{Pt^{2+}}$ in the ionomer of the catalyst layer, which is

described by the differential equation:

$$\varepsilon_{i,CL} \frac{dc_{Pt^{2+}}}{dt} = 4\pi \sum ((r^i)^2 n^i R_{diss}^i), \quad (11)$$

where $\varepsilon_{i,CL}$ is the ionomer volume fraction in the CL.

Small particles are more prone to dissolution, which is described using a constant surface energy σ_{Pt} :

$$E_{diss}^{eq,i} = E_{diss}^{eq,bulk} - \frac{\sigma_{Pt} M_{Pt}}{2r^i \rho_{Pt} F}. \quad (12)$$

There seems to be a confusion about the radius dependency of the equilibrium potential for platinum dissolution in literature. Since the value for σ_{Pt} is taken from Darling and Meyers (2003), their formulation is used, too. However, one can find a factor of 2 or 3 in the numerator in different publications (Bi and Fuller 2008; Holby and Morgan 2012; Kaptay 2017; Jahnke et al. 2020).

The radius of the particle group i either shrinks or grows due to the dissolution rate R_{diss} , which adds another differential equation per particle group to the system of ordinary differential equations (ODEs):

$$\frac{dr^i}{dt} = \frac{-M_{Pt}}{\rho_{Pt}} R_{diss}^i. \quad (13)$$

All in all, the model has initially $n+2$ differential states where $n=20$ is the chosen number of initial particle groups (see above). The translated model has no nonlinear system to solve. Table 3 lists all differential states including the chosen nominal value within a typical range for that state.

Using the described radial evolution approach, smaller particles are getting smaller until they disappear. Since the equilibrium potential for platinum dissolution (equation 12) goes to negative infinity for a radius of zero, a minimum valid radius r_{min} is defined and set to 0.45 nm. If the radius of a particle group reaches this value, an event is triggered and the particles “disappear”. Thus, the radius is set to zero and an integer in the trigger vector is set to zero which deactivates the corresponding equations, i.e. equation 12 and 13 for the that particle group.

Listing 1. Event indicating and handling

```

for i in 1:n_groups loop
  when r[i] < r_min then
    reinit(r[i], 0);
    trigger[i] = 0;
  end when;
end for;
    
```

Degradation phenomena are typically measured in accelerated stress tests (ASTs). Such an AST is simulated for a temperature of 80 °C, a relative humidity of 80 % and an electric potential symmetrically changing within 0.5 s between a lower potential limit (LPL) of 0.6 V and an upper potential limit (UPL) of 0.95 V in a period of 5 s. The simulation was performed with the *DASSL* solver and a tolerance of 10^{-4} . Figure 4 shows the result for a

Table 1. Equations used to describe the reaction rates of platinum oxidation and dissolution

$$R_{\text{PtO}} = k_{\text{PtO}} \left[\exp\left(\frac{-\omega_{\text{PtO}} \theta_{\text{PtO}}}{RT}\right) \exp\left(\frac{\alpha_{\text{PtO,ox}} z_{\text{PtO}} F}{RT} (E - E_{\text{PtO}}^{\text{eq}})\right) - \theta_{\text{PtO}} \left(\frac{c_{\text{H}^+}}{c_{\text{ref}}}\right)^2 \exp\left(\frac{-\alpha_{\text{PtO,red}} z_{\text{PtO}} F}{RT} (E - E_{\text{PtO}}^{\text{eq}})\right) \right] \quad (7)$$

$$R_{\text{diss}}^i = k_{\text{diss}} \theta_{\text{av}} \left[\exp\left(\frac{\alpha_{\text{diss,ox}} z_{\text{diss}} F}{RT} (E - E_{\text{diss}}^{\text{eq},i})\right) - \left(\frac{c_{\text{Pt}^{2+}}}{c_{\text{ref}}}\right) \exp\left(-\frac{\alpha_{\text{diss,red}} z_{\text{diss}} F}{RT} (E - E_{\text{diss}}^{\text{eq},i})\right) \right] \quad (8)$$

Table 2. Parameter of the catalyst degradation model

Parameter	Description	Value	Unit	Literature
c_{ref}	Reference concentration	1×10^{-3}	mol m^{-3}	Darling and Meyers (2003)
$E_{\text{diss}}^{\text{eq,bulk}}$	Equilibrium potential	1.188	V	Darling and Meyers (2003)
$E_{\text{PtO}}^{\text{eq}}$	Equilibrium potential	0.765 †	V	Darling and Meyers (2003)
EW	Equivalent weight of the ionomer	1.1	kg mol^{-1}	
F	Faraday constant	96,485.33	A s mol^{-1}	
k_{diss}	Reaction constant	3×10^{-6}	$\text{mol m}^{-2} \text{s}^{-1}$	Bi and Fuller (2008)
k_{PtO}	Reaction constant	7×10^{-6}	$\text{mol m}^{-2} \text{s}^{-1}$	Bi and Fuller (2008)
M_{Pt}	Molar mass	195×10^{-3}	kg mol^{-1}	Darling and Meyers (2003)
$M_{\text{H}_2\text{O}}$	Molar mass	18.02×10^{-3}	kg mol^{-1}	
R	Molar gas constant	8.314	$\text{J mol}^{-1} \text{K}^{-1}$	
z_{diss}	Number of electrons	2	1	Darling and Meyers (2003)
z_{PtO}	Number of electrons	2	1	Darling and Meyers (2003)
$\alpha_{\text{diss,ox}}$	Transfer coefficient	0.5	1	Darling and Meyers (2003)
$\alpha_{\text{diss,red}}$	Transfer coefficient	0.5	1	Darling and Meyers (2003)
$\alpha_{\text{PtO,ox}}$	Transfer coefficient	0.4	1	Bi and Fuller (2008)
$\alpha_{\text{PtO,red}}$	Transfer coefficient	0.1	1	Bi and Fuller (2008)
Γ	Number of active sites	2.18×10^{-5}	mol m^{-2}	Darling and Meyers (2003)
$\varepsilon_{\text{i,CL}}$	Ionomer volume fraction	0.3	1	Bi and Fuller (2008)
$\rho_{\text{i,dry}}$	Density	2×10^3	kg m^{-3}	
ρ_{Pt}	Density	21.45×10^3	kg m^{-3}	Darling and Meyers (2003)
σ_{Pt}	Surface energy	2.37	J mol^{-1}	Darling and Meyers (2003)
ω_{PtO}	Interaction parameter	30×10^3	J mol^{-1}	Darling and Meyers (2003)

† Takes into account particle size effect according to Darling and Meyers (2003) for a constant particle radius of 2 nm.

Table 3. Differential states

State	Unit	Nom.	Description
θ_{PtO}	1	1	Platinum oxide coverage
$c_{\text{Pt}^{2+}}$	mol m^{-3}	10^{-3}	Platinum ion concentration
r^i	m	10^{-9}	Radius of particles in group i

simulation over 500 operating hours. In figure 4 (a), the evolution of the radii can be seen. Smaller particles are getting smaller and finally disappear, while larger particles are getting larger. The color bar indicates the initial radii of the particle groups. The electrochemical Ostwald ripening leads to a reduced catalyst surface, which is shown in figure 4 (b) expressed as the roughness factor rf . The kinks are due to the discretization of the PSD. After 500 h of AST, over 70 % of the initial catalyst surface is lost. This

leads to a decrease of cell voltage and, thus, efficiency of the fuel cell (both not part of the model).

The loss of electrochemical surface area shown in figure 4 (b) has the typical characteristic of an high initial loss followed by a slower degradation, since the platinum particles radii has increased. Both, qualitative curvature and quantitative loss is comparable to the available literature mentioned in section 1. Nevertheless, for quantitative statements the model parameters in table 2 needs to be fitted to measurement data.

3 Numerical Analysis

The described irreversible catalyst degradation occurs over several hundreds or thousand of hours. Thus, the model should be much faster than real-time for its usage, e.g. in prognostic and health management (PHM) or for the optimization of operating conditions regarding

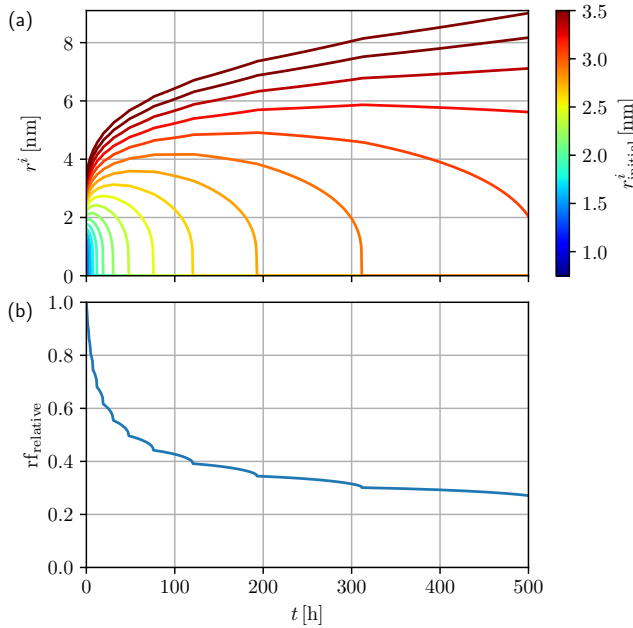


Figure 4. Simulation result for an AST over 500 hours. (a) Radial evolution. (b) Loss of electrochemical surface area expressed as roughness factor.

lifetime. A numerical analysis of the model may help to identify differential equations that slow down the simulation and find more efficient numerical formulations.

For that purpose, the linearized state space formulation is used:

$$\frac{dx}{dt} = \mathbf{A}x + \mathbf{B}u, \quad (14)$$

where \mathbf{A} is the state or system matrix, \mathbf{B} is the input matrix, \mathbf{x} is called state vector and \mathbf{u} is called input vector (Brenan, La Campbell, and Linda Ruth Petzold 1996).

For the described model using SI-units, the typical values of the differential states differ by several orders of magnitude. Visualizing \mathbf{A} could be misleading since high absolute values are only due to the dimensions. E.g., a change in particle radius would have a massive impact on platinum ion concentration, since the particle radii are in the range of 1×10^{-9} (m) and concentration in the range of 1×10^{-3} (mol m^{-3}). That is why the state space system is normalized with respect to the nominal values n_i of the states (see table 3) and a typical height for a changing input h_i :

$$\begin{pmatrix} \frac{\dot{x}_1}{n_1} \\ \vdots \\ \frac{\dot{x}_n}{n_n} \end{pmatrix} = \begin{pmatrix} a_{11} & \dots & a_{1n} \frac{n_n}{n_1} \\ \vdots & \ddots & \vdots \\ a_{n1} \frac{n_1}{n_n} & \dots & a_{nn} \end{pmatrix} \begin{pmatrix} \frac{x_1}{n_1} \\ \vdots \\ \frac{x_n}{n_n} \end{pmatrix} + \begin{pmatrix} b_{11} \frac{h_1}{n_1} & \dots & b_{1n} \frac{h_n}{n_1} \\ \vdots & \ddots & \vdots \\ b_{n1} \frac{h_1}{n_n} & \dots & b_{nn} \frac{h_n}{n_n} \end{pmatrix} \begin{pmatrix} \frac{u_1}{h_1} \\ \vdots \\ \frac{u_n}{h_n} \end{pmatrix}. \quad (15)$$

The input heights were chosen to $h_E = 0.1$ V and $h_T = 10$ K for the electrical potential and temperature at the CL, respectively. Neither the diagonal entries of matrix \mathbf{A} nor the eigenvalues change due to this normalization.

The model was linearized and analyzed at typical conditions, i.e. an electric potential of 0.85 V, a temperature of 80 °C and a relative humidity of 80 % after reaching quasi-equilibrium using the “full linear analysis” method in *Dymola 2023x* and the *Modelica_LinearSystems2* package (DLR Institute of System Dynamics and Control 2020). Note, that due to degradation and the changing PSD no true equilibrium is reached.

Figure 5 shows a graphic visualization of the system matrix \mathbf{A} and input matrix \mathbf{B} . Dark gray is associated with a high absolute value, white are values close to zero or zero. Positive values are additionally marked as blue. Both matrices can be interpreted as follows: The column marks the changing variable (differential state in \mathbf{A} or input in \mathbf{B}) and the row marks the normalized change of derivative. The higher the value (dark gray), the higher the absolute impact of the changing variable on the state derivative. Exemplary, all radii have a relatively high impact on the derivation of the platinum ion concentration but no impact on the oxide coverage, since the oxide coverage does not depend on the particle radii (see section 2). However, the oxide coverage has an impact on the derivation of the radii. The impact is positive for small radii (marked as blue), since an increased oxide coverage leads to a reduced electrochemical dissolution and, thus, to a less negative change of particle radii (see equation 8). The largest absolute value on the main diagonal corresponds to the platinum ion concentration, indicating that this state has the smallest time constant.

In matrix \mathbf{B} , the big impact of the electrical potential on all differential states can be seen. As expected and later further discussed, the impact on platinum ion concentration and oxide coverage is much higher than on the particle radii, since latter are changing much slower due to degradation.

The matrix \mathbf{A} can be used to determine the eigenvalues λ of the system, since they are the root of

$$[\lambda \mathbf{I} - \mathbf{A}] \mathbf{x} = 0 \quad (16)$$

with the identity matrix \mathbf{I} . The *eigvals-method* from *Scipy* in python is used to determine λ .

Table 4 lists the extracted eigenvalues and time constants τ . They are sorted and numbered from smallest to largest time constant. The eigenvalues can be interpreted as follows: Number one is associated with the platinum ion concentration in the ionomer. Number two is associated with the platinum oxide coverage. All others can be interpreted as the particle radii changing due to degradation. This irreversible degradation phenomena is very slow compared to the fast changing platinum ion concentration and the platinum oxide coverage. Hence, the time constants are much higher. However, for a system matrix \mathbf{A} that is no triangular matrix, the contribution of the

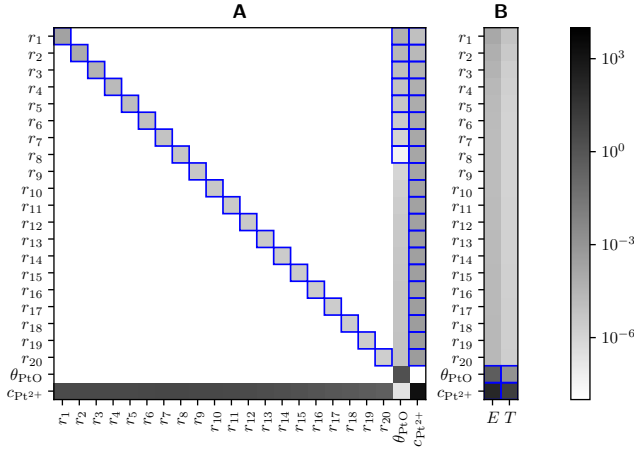


Figure 5. Visualization of the normalized matrices **A** and **B**. Absolute values of matrix entries are used for color bar. Positive values are marked blue.

eigenvalue to the continuous states is not unambiguously. Since 19 out of 22 eigenvalues are positive, the linearized system is not stable.

Table 4. Eigenvalues and time constants τ of the degradation model with dynamic platinum ion concentration

#	associated	Eigenvalue	τ [s]
1	$c_{\text{Pt}^{2+}}$	-1.5×10^3	6.7×10^{-4}
2	θ_{PtO}	-1.7	6.0×10^{-1}
3	r^i	2.5×10^{-4}	4.0×10^3
...	r^i
21	r^i	2.1×10^{-6}	4.7×10^5
22	r^i	-1.6×10^{-6}	6.3×10^5

The ratio from largest to smallest eigenvalue is around 10^9 . This large ratio indicates that the system of ODEs is a so called “stiff system” (T. D. Bui and T. R. Bui 1979). The problem of “stiffness” is discussed in literature for several decades. Nevertheless, there is no clear mathematical definition of “stiffness” (Hairer and Wanner 1991). It is typically defined as a system where explicit methods do not work or implicit methods are tremendously better (Curtiss and Hirschfelder 1952; Ascher and Linda R. Petzold 1998). In this work, we use the ratio from largest to smallest eigenvalue to quantify the “stiffness”.

Another way to quantify the contribution of the different states to the numerical effort is the analysis of the *states which dominate error* or *limits step size* during integration. Values extracted from *Dymola 2023x* for the previously described simulation (figure 4) are listed in table 5. It can be seen that the platinum ion concentration in the ionomer $c_{\text{Pt}^{2+}}$ dominates the error and is limiting the step size.

Table 5. Contribution of the different states to the numerical effort

state	limits step size [%]	dominates error [%]
θ_{PtO}	0.03	9.07
$c_{\text{Pt}^{2+}}$	99.97	90.93
$\sum r^i$	0.00	0.00

4 Increasing Simulation Speed

The platinum ion concentration in the ionomer limits the step size and, thus, slows down the simulation. This can be explained with the very small time constant of the corresponding state, c.f. table 4. It is much smaller than the typical excitation signal, i.e. the change of temperature, electrical potential or relative humidity in the CL. Hence, we propose that it should be treated to be in quasi-equilibrium.

The left side of equation 11 is set to zero to calculate the platinum ion concentration in quasi-equilibrium:

$$0 = 4\pi \sum ((r^i)^2 n^i R_{\text{diss}}^i). \quad (17)$$

The explicit formulation

$$c_{\text{Pt}^{2+}} = \frac{\sum \left[(r^i)^2 n^i \exp \left(\frac{\alpha_{\text{diss,ox}} z_{\text{diss}} F}{RT} (E - E_{\text{diss}}^{\text{eq},i}) \right) \right]}{\sum \left[\frac{(r^i)^2 n^i}{c_{\text{ref}}} \exp \left(-\frac{\alpha_{\text{diss,red}} z_{\text{diss}} F}{RT} (E - E_{\text{diss}}^{\text{eq},i}) \right) \right]} \quad (18)$$

does not need to be implemented since Modelica can handle implicit formulations but might help others to implement it in programming languages that need explicit formulations. Note, that diffusion of platinum ions into the membrane (Pt-band) using Fick’s law of diffusion can be easily integrated in equation 18. The new model uses equation 17 instead of equation 11. Thus, the model has $n + 1$ differential states and still no nonlinear system of equations.

Figure 6 shows a comparison between the “classic” formulation where the platinum ion concentration is a differential state and the new formulation where the concentration is analytically calculated in quasi-equilibrium. At $t = 2$ s, the electric potential is jumping from 0.6 V to 0.95 V and at $t = 4$ s back to 0.6 V, c.f. figure 6 (a). Figure 6 (b) shows the increasing platinum oxide coverage. The time constant in the sub-second range can be seen, c.f. eigenvalue 2 in table 4. Due to platinum dissolution, the ion concentration suddenly increases (figure 6 (c)). Only a small deviation between the two variants can be seen, visualizing the very small time constant for the platinum ion concentration. The slight increase in concentration between $t = 2$ s and $t = 4$ s is due to irreversible degradation, i.e. the changing PSD.

Note, that a potential jump is the scenario with the highest deviation between both variants. Typically, the potential is changing ramp-like within a second or more. Nevertheless, even for the case with potential jumping

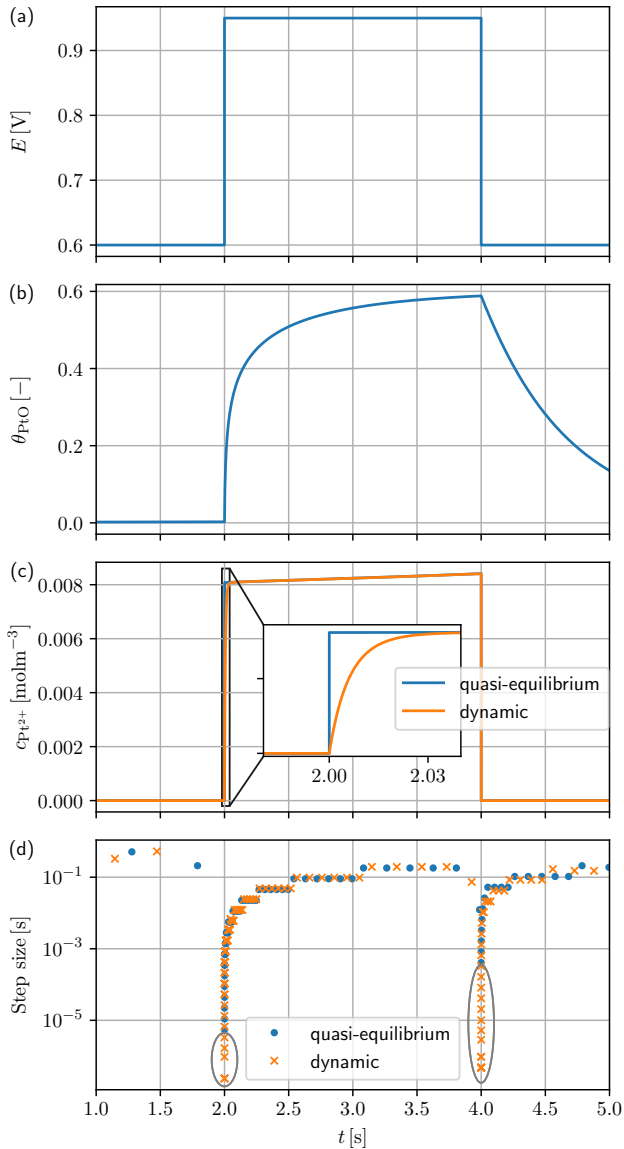


Figure 6. Comparison between the variant with platinum ion concentration in the ionomer as a differential state (orange) and in quasi-equilibrium (blue). (a) shows the electric potential, (b) shows the platinum oxide coverage (same for both variants), (c) shows the platinum ion concentration and (d) shows the steps sizes.

from 0.6 V to 0.95 V and vice versa every 2 s, the rf-loss (loss of electrochemical surface area) after 500 hours differs less than 0.1 % between both variants (not shown).

Figure 6 (d) shows the step sizes used for integration by *DASSL*. It can be seen that the step size is much smaller for the variant where platinum ion concentration is a differential state, especially after the decreasing potential at $t = 4$ s. Fast and large changes in electric potential with the “classic” formulation were also leading to situations where the platinum ion concentration did not converge for the minimum allowed step size. Those problems did not occur with the new formulation.

By calculating the platinum ion concentration in the ionomer in quasi-equilibrium it is possible to get rid of the smallest time constant and decrease the systems “stiffness”. The ratio from largest to smallest time constant can be reduced from 9.4×10^8 to 1.1×10^6 . This helps to increase simulation speed and numerical robustness meaning less problems with convergence.

To quantify the increase of simulation speed, a real-time factor is introduced as the ratio of simulation time and CPU-time. The higher the real-time factor, the faster the simulation. All simulations were performed on a personal laptop computer with an AMD Ryzen 7 PRO 4750U (Base Clock 1.7 GHz). The CPU-time and, thus, the real-time factor, varies due to other processes on the computer and, since a solver with variable step size is used, on the chosen step sizes. The chosen steps are the same for each repeated identical simulation but can vary dramatically for different parameters or inputs. Therefore, 1,000 Monte-Carlo simulations are performed with different AST-profiles. A shape-factor is randomly chosen between 0 (square wave signal) and 1 (triangular wave). LPL is varied between 0.4 V and 0.7 V, UPL between 0.8 V and 1.2 V. The period of 5 s is kept constant for a simulation time of 1 h. Again, *DASSL* with a tolerance of 10^{-4} is used.

Figure 7 shows a comparison of the simulation speed for both variants. The thickness of the violin plots indicates the density of occurrence. The differences in simulation speed within one variant is mainly due to the variation of the potential profile. The variant with platinum ion concentration in quasi-equilibrium is much faster. The simulation time is nearly proportional to the number of F-evaluations (not shown), i.e. evaluations of the right hand side (RHS) of the hybrid ODE. This indicates, again, that larger step sizes are possible due to the quasi-equilibrium formulation. In all 1,000 simulated cases, the variant with platinum ion concentration in quasi-equilibrium is faster than the dynamic variant (not shown). The average real-time factor was more than doubled ending in a factor of approximately 1,260. Thus, 500 hours of AST can be simulated within 23 minutes.

5 Summary and Discussion

A fast and efficient catalyst degradation model for PEMFC was introduced using the multi-physics modeling lan-

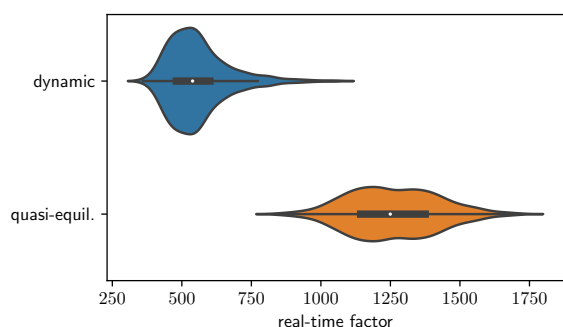


Figure 7. Real-time factor, i.e. the ratio of simulated time and CPU-time, for the variants with dynamic platinum ion concentration and concentration in quasi-equilibrium. The thickness of the violin plots indicates the density of occurrence.

guage Modelica. The model, predominantly based on Darling and Meyers (2003), can describe platinum oxide formation, platinum dissolution and, thus, electrochemical Ostwald ripening and the reduction of catalyst surface area.

Using the state space formulation, the system matrix **A** and the input matrix **B** were discussed and the eigenvalues respectively time constants were extracted. The problem of “stiffness” for this type of degradation model was discussed, meaning a tremendous difference in time constants. It was shown, that the time constant for the platinum ion concentration in the ionomer is much lower than the typical excitation signal, i.e. the change of the inputs temperature and electrical potential. Calculating the platinum ion concentration explicit in quasi-equilibrium removes the differential state with the smallest time constant, reduces “stiffness” and increases simulation speed without creating a nonlinear system of equations or relevant inaccuracies. Using the new formulation, the simulation speed could be more than doubled ending in an average real-time factor for a typical AST of over 1,000. Thus, 500 hours of AST can be simulated within less than 30 minutes which allows the usage of the model for extensive parameter studies, PHM and optimization, e.g. regarding the operating conditions.

References

- Ahluwalia, Rajesh K., Srikanth Arisetty, Jui-Kun Peng, et al. (2014). “Dynamics of Particle Growth and Electrochemical Surface Area Loss due to Platinum Dissolution”. In: *Journal of The Electrochemical Society* 161.3, F291–F304. ISSN: 0013-4651. DOI: 10.1149/2.051403jes.
- Ahluwalia, Rajesh K., Srikanth Arisetty, Xiaoping Wang, et al. (2013). “Thermodynamics and Kinetics of Platinum Dissolution from Carbon-Supported Electrocatalysts in Aqueous Media under Potentiostatic and Potentiodynamic Conditions”. In: *Journal of The Electrochemical Society* 160.4, F447–F455. ISSN: 0013-4651. DOI: 10.1149/2.018306jes.
- Ascher, Uri M. and Linda R. Petzold (1998). *Computer methods for ordinary differential equations and differential-algebraic equations*. Philadelphia: Society for Industrial and Applied Mathematics. ISBN: 9780898714128.
- Bernhard, David et al. (2023). “Model-assisted analysis and prediction of activity degradation in PEM-fuel cell cathodes”. In: *Journal of Power Sources* 562, p. 232771. DOI: 10.1016/j.jpowsour.2023.232771.
- Bi, Wu and Thomas F. Fuller (2008). “Modeling of PEM fuel cell Pt/C catalyst degradation”. In: *Journal of Power Sources* 178.1, pp. 188–196. DOI: 10.1016/j.jpowsour.2007.12.007.
- Borup, Rodney L. et al. (2020). “Recent developments in catalyst-related PEM fuel cell durability”. In: *Current Opinion in Electrochemistry* 21, pp. 192–200. ISSN: 24519103. DOI: 10.1016/j.coelec.2020.02.007.
- Brenan, Kathryn Eleda, Stephen Vern La Campbell, and Linda Ruth Petzold (1996). *Numerical solution of initial-value problems in differential-algebraic equations*. Vol. 14. Classics in applied mathematics. Philadelphia: Society for Industrial and Applied Mathematics. ISBN: 0898713536.
- Bui, T. D. and T. R. Bui (1979). “Numerical methods for extremely stiff systems of ordinary differential equations”. In: *Applied Mathematical Modelling* 3.5, pp. 355–358. ISSN: 0307-904X. DOI: 10.1016/S0307-904X(79)80042-6. URL: <https://www.sciencedirect.com/science/article/pii/S0307904X79800426>.
- Curtiss, C. F. and J. O. Hirschfelder (1952). “Integration of Stiff Equations”. In: *Proceedings of the National Academy of Sciences of the United States of America* 38.3, pp. 235–243. ISSN: 0027-8424. DOI: 10.1073/pnas.38.3.235.
- Darling, Robert M. and Jeremy P. Meyers (2003). “Kinetic Model of Platinum Dissolution in PEMFCs”. In: *Journal of The Electrochemical Society* 150.11, A1523. ISSN: 0013-4651. DOI: 10.1149/1.1613669.
- Darling, Robert M. and Jeremy P. Meyers (2005). “Mathematical Model of Platinum Movement in PEM Fuel Cells”. In: *Journal of The Electrochemical Society* 152.1, A242. ISSN: 0013-4651. DOI: 10.1149/1.1836156.
- DLR Institute of System Dynamics and Control (2020). *Modelica Linear Systems 2*.
- European Union (2021). *Regulation (EU) 2021/1119 of the European Parliament and of the Council of 30 June 2021 establishing the framework for achieving climate neutrality and amending Regulations (EC) No 401/2009 and (EU) 2018/1999 (‘European Climate Law’)*: PE/27/2021/REV/1. URL: <http://data.europa.eu/eli/reg/2021/1119/oj>.
- Greszler, Thomas A., David Caulk, and Puneet Sinha (2012). “The Impact of Platinum Loading on Oxygen Transport Resistance”. In: *Journal of The Electrochemical Society* 159.12, F831–F840. ISSN: 0013-4651. DOI: 10.1149/2.061212jes.
- Hairer, Ernst and Gerhard Wanner (1991). *Solving Ordinary Differential Equations II: Stiff and Differential-Algebraic Problems*. Vol. 14. Springer eBook Collection Mathematics and Statistics. Berlin, Heidelberg: Springer. ISBN: 978-3-662-09949-0. DOI: 10.1007/978-3-662-09947-6.
- Holby, Edward F. and Dane Morgan (2012). “Application of Pt Nanoparticle Dissolution and Oxidation Modeling to Understanding Degradation in PEM Fuel Cells”. In: *Journal of The Electrochemical Society* 159.5, B578–B591. ISSN: 0013-4651. DOI: 10.1149/2.011204jes.
- Jahnke, Thomas et al. (2020). “Physical Modeling of Catalyst Degradation in Low Temperature Fuel Cells: Platinum Oxidation, Dissolution, Particle Growth and Platinum Band Formation”. In: *Journal of The Electrochemical Society* 167.1, p. 013523. ISSN: 0013-4651. DOI: 10.1149/2.0232001JES.

- Kaptay, George (2017). “A new paradigm on the chemical potentials of components in multi-component nano-phases within multi-phase systems”. In: *RSC Advances* 7.65, pp. 41241–41253. DOI: 10.1039/C7RA07911G.
- Kregar, Ambrož et al. (2019). “Predictive virtual modelling framework for performance and platinum degradation modelling of high temperature PEM fuel cells”. In: *Energy Procedia* 158, pp. 1817–1822. ISSN: 18766102. DOI: 10.1016/j.egypro.2019.01.426.
- Li, Yubai et al. (2015). “A One-Dimensional Pt Degradation Model for Polymer Electrolyte Fuel Cells”. In: *Journal of The Electrochemical Society* 162.8, F834–F842. ISSN: 0013-4651. DOI: 10.1149/2.0101508jes.
- Prokop, M. et al. (2019). “Degradation kinetics of Pt during high-temperature PEM fuel cell operation part I: Kinetics of Pt surface oxidation and dissolution in concentrated H₃PO₄ electrolyte at elevated temperatures”. In: *Electrochimica Acta* 313, pp. 352–366. ISSN: 00134686. DOI: 10.1016/j.electacta.2019.04.144.
- Rinaldo, Steven G., Jürgen Stumper, and Michael Eikerling (2010). “Physical Theory of Platinum Nanoparticle Dissolution in Polymer Electrolyte Fuel Cells”. In: *The Journal of Physical Chemistry C* 114.13, pp. 5773–5785. ISSN: 1932-7447. DOI: 10.1021/jp9101509.
- Schneider, Patrick et al. (2019). “Fast and Reliable State-of-Health Model of a PEM Cathode Catalyst Layer”. In: *Journal of The Electrochemical Society* 166.4, F322–F333. ISSN: 0013-4651. DOI: 10.1149/2.0881904jes.
- Shao-Horn, Y. et al. (2007). “Instability of Supported Platinum Nanoparticles in Low-Temperature Fuel Cells”. In: *Topics in Catalysis* 46.3-4, pp. 285–305. ISSN: 1022-5528. DOI: 10.1007/s11244-007-9000-0.
- Springer, T. E., T. A. Zawodzinski, and S. Gottesfeld (1991). “Polymer Electrolyte Fuel Cell Model”. In: *Journal of The Electrochemical Society* 138.8, pp. 2334–2342. DOI: 10.1149/1.2085971.
- Wagner, Carl (1961). “Theorie der Alterung von Niederschlägen durch Umlösen (Ostwald-Reifung)”. In: *Zeitschrift für Elektrochemie, Berichte der Bunsengesellschaft für physikalische Chemie* 65.7–8, pp. 581–591. ISSN: 0005-9021. DOI: 10.1002/bbpc.19610650704.
- Zhang, Hao et al. (2013). “The Impact of Potential Cycling on PEMFC Durability”. In: *Journal of The Electrochemical Society* 160.8, F840–F847. ISSN: 0013-4651. DOI: 10.1149/2.083308jes.
- Zihrul, Patrick et al. (2016). “Voltage Cycling Induced Losses in Electrochemically Active Surface Area and in H₂/Air-Performance of PEM Fuel Cells”. In: *Journal of The Electrochemical Society* 163.6, F492–F498. ISSN: 0013-4651. DOI: 10.1149/2.0561606jes.

where the parameter n_0 describes the absolute amount of platinum particles

$$n_0 = \frac{L_{\text{Pt}}}{\sum_{i=1}^n \frac{4}{3}\pi(r^i)^3 n^i t_{\text{cl}} \rho_{\text{Pt}}}. \quad (20)$$

The parameter for the distribution $\ln(\mu) = 1.58 \times 10^{-9} \text{ m}$, $\sigma = 0.31$, $t_{\text{cl}} = 20 \mu\text{m}$ and $L_{\text{Pt}} = 0.6 \text{ mg cm}^{-2}$ are taken from Jahnke et al. (2020). The resulting geometric surface area is $71.2 \text{ m}^2 \text{ g}^{-1}$.

A Initial Particle Size Distribution

The initial PSD (figure 3) is approximated using 20 particle groups with equidistant distributed radii between 0.75 nm and 3.5 nm and a log-normal distribution

$$n^i = \frac{n_0}{r^i \sigma \sqrt{2\pi}} \exp\left(-\frac{(\ln(r_i) - \mu)^2}{2\sigma^2}\right), \quad (19)$$